0.1 Defining the model

The rotation of a rigid body in the rotating reference frame is described by Euler's equations. To derive these, we begin with Euler's second law for the angular momentum **L** in the interial frame

$$\frac{d\mathbf{L}}{dt} = \mathbf{T}, \tag{0.1.1}$$

where **T** is the applied torque. The angular momentum can be written as $I\boldsymbol{\omega}$, the product of the moment of interia tensor and the spin vector. In the inertial frame both of these quantities vary in time; this does not lend itself to solving the equations. We can simplify solutions by transforming to a frame fixed in the rotating frame of the rigid body and aligning the axes with the principle axes of I. In such as frame the moment of inertia is constant and diagonal. The transformation to a rotating reference frame requires a modification of the time derivative in Euler's second law, see Landau and Lifshitz (1969) for details. The result is Euler's rigid body equations in the rotating frame:

$$\frac{d\mathbf{L}}{dt} + \boldsymbol{\omega} \times \mathbf{L} = \mathbf{T}. \tag{0.1.2}$$

To begin with, we will restrict ourselves to consider only biaxial bodies with principle moments given by

$$I_x = I_y = I_0 \qquad I_z = I_0(1 + \epsilon_I), \tag{0.1.3}$$

where I_0 is the moment of inertia for which we use a canonical value of

$$I_0 = \frac{2}{5}MR^2 \approx 10^{45} \text{g cm}^2 M_{1.4} R_6^2.^{[1]} \tag{0.1.4}$$

Equation 0.1.2 gives us three coupled ODEs for ω_x, ω_y and ω_z. In the torque-free case analytic solutions can be found. If the spin-vector is initially at some angle to the $\hat{\boldsymbol{z}}$ axes, it will rotate in a cone about the $\hat{\boldsymbol{z}}$ axes. This motion in referred to as free precession and the period is given by

$$\tau_p = \frac{1}{\epsilon_I \nu_0}, \tag{0.1.5}$$

where $\nu_0 = \omega_0/2\pi$ is the initial spin frequency.

We now will not include a torque modelling a dipole m frozen into the star in the $\hat{\boldsymbol{x}} - \hat{\boldsymbol{z}}$ plane at an angle χ to the $\hat{\boldsymbol{z}}$ axis. Deutsch (1955) demonstrated such a dipole exerts a torque on the star which has two components. It is presented here in form found in Goldreich (1970, hereafter G70).

$$\boldsymbol{T} = \frac{2R}{3c} I_0 \epsilon_A \omega^2 (\boldsymbol{\omega} \times \hat{\boldsymbol{m}}) \times \hat{\boldsymbol{m}} + \epsilon_A I_0 (\boldsymbol{\omega} \cdot \hat{\boldsymbol{m}})(\boldsymbol{\omega} \times \hat{\boldsymbol{m}}), \quad \text{with} \quad \epsilon_A = \frac{m^2}{I_0 R_6 c^2}, \tag{0.1.6}$$

where ϵ_A the magnetic deformation as defined by Glampedakis and Jones (2010). The first term on the right hand side is often referred to as the *spin down*, or *braking* torque. As this suggests it is responsible for the power law retardation of spin frequency and has

---

[1] $M_{1.4}$ is mass in units of $1.4 M_\odot$ and R_6 is the radius in units of 10^6cm

an associated timescale τ_S. The second term is known as the *anomalous* torque which acts on a timescale τ_A. These time scales are given by

$$\tau_A = \frac{1}{\epsilon_A \nu_0}, \qquad \tau_S = \frac{3c}{2R} \frac{1}{\epsilon_A \nu_0^2}, \tag{0.1.7}$$

We now have the basic components of out neutron star: a biaxial rigid body spundown by a dipole torque. In table 0.1.1 we list the relevant angles of each component and a sketch is provides in figure 0.1.1.

		Magnitude	Polar angle	Azimuthal angle
Spin vector	$\boldsymbol{\omega}$	ω	a	ϕ
Magnetic dipole	$\boldsymbol{m}$	m	χ	0

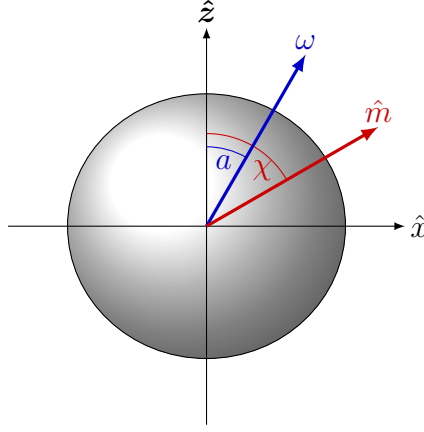Table 0.1.1: Table of spherical components for the spin vector and magnetic dipole

Figure 0.1.1: Sketch of the $\hat{\boldsymbol{x}} - \hat{\boldsymbol{z}}$ plane, the magnetic dipole lies solely in this plane, it's azimuthal component is always zero. Only the projection into this plane of the spin vector is shown, in general it has an azimuthal component given by ϕ.

We will now present results of this model found using numerical intergration of (0.1.2) with the torque defined in (0.1.6).

0.2 Spherical star

As a first validation that the model agrees with analytic calculations we solve for a spherical star $\epsilon_I = 0$. In such a case the star will not precess. This model was first considered by Davis and Goldstein (1970) and separately by Michel and Goldwire (1970); both sets of authors discovered that the spin axis aligns with the magnetic axis on the spindown timescale. This is incompatible with the observation of neutron stars as NSs as we need the dipole to be misaligned with the spin axes to observe pulses.

We set $\chi = 30°$ and $\epsilon_A = 5 \times 10^{-11}$ and plot the components of the spherical components spin vector in figure 0.2.1. This shows a brief spin down which halts once the

spin vector aligns with the magnetic dipole $a \to \chi = 30°$. The azimuthal angle ϕ does not vary, this is expected since precession, a monotonic increase in ϕ, does not occur for spherical bodies. This result agrees with the analytic calculations: the allignment occurs on the spin down time scale $\sim 3.6 \times 10^8$.
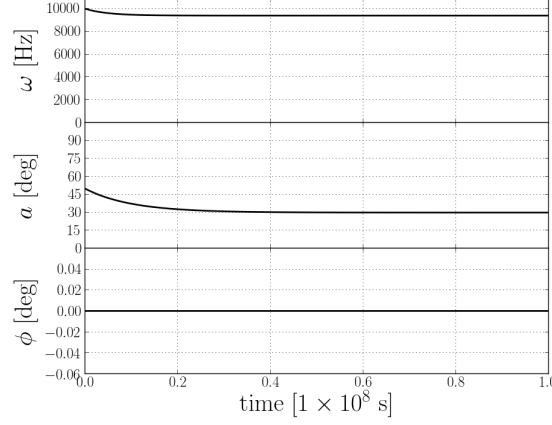

Figure 0.2.1: Plot of the spherical components of $\boldsymbol{\omega}$ for a spherical star. Note that the magnetic dipole is inclined at $\chi = 30°$ to the $\hat{\boldsymbol{z}}$ axis.

0.3 Biaxial NS with no anomalous torque

We begin with the evolution of the spin vector neglecting the anomalous torque. This reduces the number of timescales to just two, the spin down and the precession timescale. The solutions are categorised by the ordering of these time scales; it is shown in appendix .B that these orderings remain valid for the duration of the spindown. The ordering of the two timescales gives three different types of solutions corresponding to three regions:

$$\text{Regions A: } \tau_S > \tau_P \qquad \text{Region B: } \tau_S \sim \tau_P \qquad \text{Resgion C: } \tau_S < \tau_P \qquad (0.3.1)$$

Since all solutions in each region display the same behaviour, we pick three 'neutron stars (NS)' and list their parameters in table 0.3.1.

	ϵ_I	ϵ_A	B_S [Gauss]	τ_S [s]	τ_P [s]
NS A	1.0×10^{-9}	0.5×10^{-10}	1.3×10^{13}	3.6×10^8	6.3×10^5
NS B	0.4×10^{-10}	0.5×10^{-10}	1.3×10^{13}	3.6×10^8	1.6×10^7
NS C	1.0×10^{-15}	0.5×10^{-10}	1.3×10^{13}	3.6×10^8	6.3×10^{11}

Table 0.3.1: Table of relevant values for the selected points. In calculating the Magnetic fields we have assumed canonical value of $R = 1 \times 10^6$cm for the radius, and a value $\omega_0 = 1 \times 10^4$ rads s^{-1}

Phase space

The phase space of solutions is plotted in figure 0.3.1 parametrised by the elastic deformation ϵ_I and the surface magnetic field B_S which is given by (Shapiro and Teukolsky, 1983, p. 278)
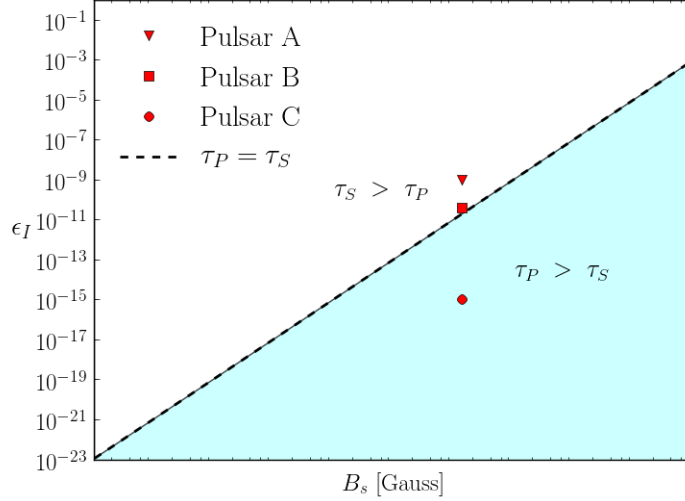
$$B_S = \frac{2m}{R^3} \qquad (0.3.2)$$

Figure 0.3.1: Phase space of solutions categorised by the ordering of the two timescales as a function of the elastic deformation ϵ_I and the surface magnetic fields B_s.

Without the anomalous torque the ordering of the timescales defines two distinct regions separated by $\tau_S = \tau_P$. To aid the speed of numerical calculation an unrealistic value of the initial spin frequency $\omega_0 = 10^4 [\text{rads } s^{-1}]$ is used. Using a more realistic value the type of solution remains the same only the time scales vary. A comparison of this phase space with the true NS population in section 0.5.

The elastic deformation ϵ_I may take either a positive or a negative values; these correspond to either an oblate or a prolate mass distribution. In all of the following we use only positive values of ϵ_I as these are thought to be more physical. It will be noted when this is thought to be important. Finally we must choose the angle between the magnetic dipole and the elastic deformations χ, because of the symmetry of the star about the $\hat{z}$ axis we choose two values 30° and 75° to demonstrate important cases. Initial conditions are thought to have some bearing on the solutions (see Melatos, 2000). In the current work we will start with the spin vector having inclination angle of 50° and azimuth 0°.

0.3.1   NS A in region $\tau_S \gg \tau_P$

NSs in this region are described by the work of G70. In addressing the shortcomings of the analytic spherical solutions, Goldreich considered a neutron star with a solid crust capable of supporting elastic strains. In order to find an analytic solution Goldreich assumed that

the precession timescale was significantly shorter than the spin down timescale. Averaging equations (0.1.2) with this assumptions yields

$$\left\langle \frac{d\omega}{dt} \right\rangle = -\frac{2R}{3c}\epsilon_a \omega^3 \left[\sin^2 \chi + \sin^2 a \left(1 - \frac{3}{2}\sin^2 \chi \right) \right], \qquad (0.3.3)$$

$$\left\langle \frac{da}{dt} \right\rangle = -\frac{2R}{3c}\epsilon_a \omega^2 \sin a \cos a \left(1 - \frac{3}{2}\sin^2 \chi \right). \qquad (0.3.4)$$

These expression indicate that the polar angle a will either grow or decay on the spindown timescale depending on whether χ was greater or less than $\approx 55°$.

We first present results for all the spherical components during the spindown in figure 0.3.2. For the angle χ we use two values $30°$ and $75°$ and find that a tends to either 0 or $\pi/2$ on the spindown timescale as suggested by G70. During this alignment, the spin magnitude decays and ϕ monotonically increases corresponding to the spin vector precessing about the $\hat{\boldsymbol{z}}$ axis.

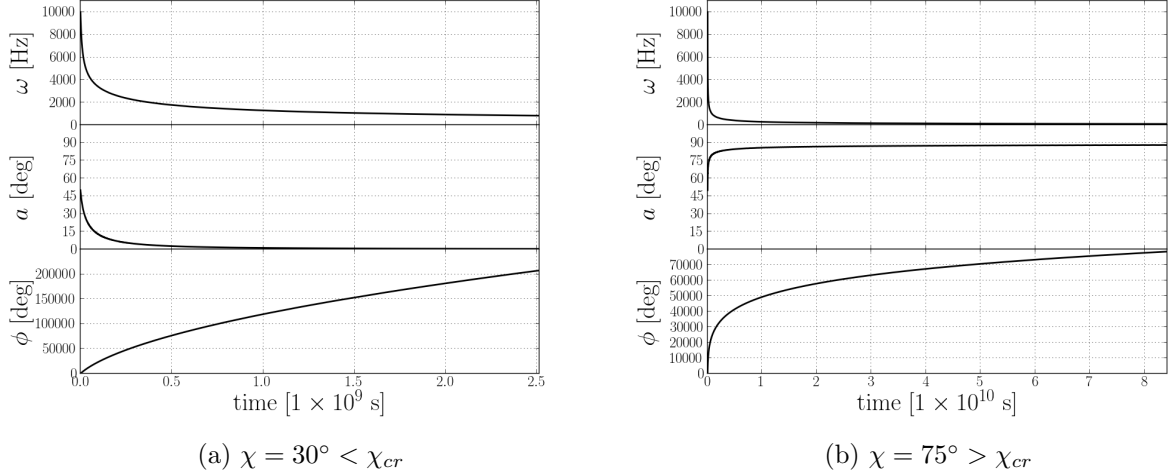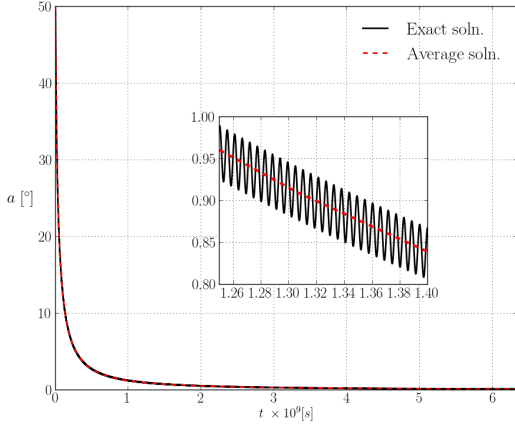(a) $\chi = 30° < \chi_{cr}$ (b) $\chi = 75° > \chi_{cr}$

Figure 0.3.2: Plot of the spherical components of $\boldsymbol{\omega}$ for NS A. The two choices of χ allow us to confirm Goldreich's dependence of the alignment of the spin vector on χ.

We investigate the differences beween Goldreich's averaged equations (0.3.4) and the exact solution without averaging in figure 0.3.3.

Our model agrees well with Goldreich's averaged result, but also exhibits oscillations due to precession.

(a) $\chi = 30° < \chi_{cr}$
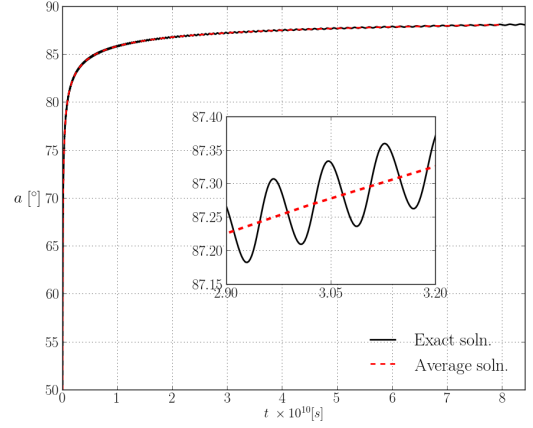
(b) $\chi = 75° > \chi_{cr}$

Figure 0.3.3: Plot of the angle a for both the exact solution of (0.1.2) and the solution to the averaged equations (0.3.4).

A geometric argument   To better understand the evolution of the spin vector and in particular the significance of $a \sim 55°$ we introduce a geometric argument. Writing the conservations of energy and momentum in terms of the angular momentum vector J_i for a biaxial mass distribution we have

$$1 = \frac{J_x^2}{2I_x E} + \frac{J_y^2}{2I_y E} + \frac{J_z^2}{2I_z E} = \frac{J_x^2}{2I_0 E} + \frac{J_y^2}{2I_0 E} + \frac{J_z^2}{2I_0(1+\epsilon_I)E}, \qquad (0.3.5)$$

$$J^2 = J_x^2 + J_y^2 + J_z^2. \qquad (0.3.6)$$

The first equation describes a biaxial ellipsoid with semi-axis given by $\sqrt{2I_0 E}$, $\sqrt{2I_0 E}$ and $\sqrt{2I_0(1+\epsilon_I)E}$. The second describes a sphere of radius J. Both shapes are concentric with their origin at $\mathbf{0}$. Physical solutions require the conservation of both the energy and momentum, these solutions are therefore the intersection of the sphere and ellipsoid. This bounds the radius of the sphere by

$$2EI_0 < J^2 < 2EI_0(1+\epsilon_I). \qquad (0.3.7)$$

For a fixed energy and momentum, the intersection describes a circle about the $\hat{\mathbf{z}}$ axis. Several typical intersections are shown in figure 0.3.4. Points on the circle are the set of all possible solutions to the conservation equations for the angular momentum vector J_i. Since $J_i = I_{ij}\omega^j$ and the moment of inertia tensor is static, numerical solutions for the spin vector must also exist as points on a related circle. This related circle is exactly the precession of $\boldsymbol{\omega}$ about the $\hat{\mathbf{z}}$ axis.

Both the energy and the momentum decay exponentially in time due to the spindown. As a result both the sphere and ellipsoid will shrink, but not necessarily at the same rate. If we imagine observing the ellipsoid such that it appears to be fixed, we may see the sphere either shrink or grow with respect to the ellipsoid. We can parameterise the relative rate of shrinking by considering the quantity

$$A(t) = \frac{J^2}{2EI_0} \qquad (0.3.8)$$

6

We could have chosen any one of the ellipsoids semi-axis since they are all proportional up to constants of ϵ_I. The evolution of the spin vector is related to the rate of change of A. This quantity determines whether the sphere shrinks or grows with respect to the ellipsoid. It is worth taking a moment to understand the different cases which are parametrised by the sign of $\dot{A}$:

1. $\dot{A} > 0$ The sphere grows with respect to the ellipsoid. In this case the intersection circles will 'close up' around the $\hat{\boldsymbol{z}}$ axis. This agrees with the solution for $\chi = 30°$ given in figure 0.3.3(a). The angle between $\boldsymbol{\omega}$ and the $\hat{\boldsymbol{z}}$ axis tends to zero while ϕ monotonically increases. This describes the spinvectors following a circle about the z axis which gradiuall decreases in radius.

2. $\dot{A} < 0$ The sphere shrinks with respect to the ellipsoid. In this case the intersection circles will increase in radius until $J \to \sqrt{2EI_0}$. This describes exactly the solution in figure 0.3.3(b): that is $a \to 90°$ while ϕ monotonically increases.
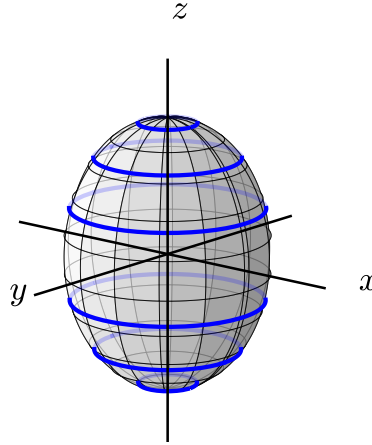

Figure 0.3.4: Intersection of the sphere and ellipsoid defined in equations (0.3.6) for three different values of M at fixed E. The sphere's of radius M are not visible, only the blue line shows where they would intersect the fixed ellipsoid.

Connecting with Goldreich's result In appendix .A we verify that the time averaged rate of change of A is given by the following.

$$\langle \dot{A} \rangle = \frac{1}{\langle E \rangle^2} I_0^2 \epsilon_I \omega^6 \frac{2R}{3c} \epsilon A \cos^2 a \sin^2 a \left(1 - \frac{3}{2} \sin^2 \chi \right) \tag{0.3.9}$$

This result is valid only in the regime for which $\tau_S \gg \tau_P$ and neglects the anomalous torque and term of order ϵ_I^2. It demonstrates that only two factors determine the sign of $\dot{A}$: the sign of ϵ_I and the term $1 - \frac{3}{2} \sin^2 \chi$ giving a critical value $\chi_{cr} \approx 55°$. The first we should expect on geometric grounds, a change in sign of the deformation changes the

geometry of the ellipsoid. The second is in perfect agreement with the findings of G70, and shows that this critical value is a tipping point between the rates of change of energy and angular momentum.

Summary   We find that, without the anomalous torque, the numerical model agrees well with analytic results in the literature. Further, we give an intepretion of the critical value of *chi* found by G70.

0.3.2   NS B in region $\tau_S \sim \tau_P$

Unlike the previous examples, there is no comparison in the literature which considers $\tau_P \sim \tau_S$ while neglecting the anomalous torque. This is primarily because the similarity of the timescales means simplifying assumptions cannot be made. The results have not been included here as they are exactly alike with the results of NS A, except the similarity of time scales means both the precession and alignment of the spin vector occur on the same timescale.

0.3.3   NS C in region $\tau_S \ll \tau_P$

In NS C the timescales take the ordering $\tau_P \gg \tau_S$. An analogy can be made that the limit of this region, is the spherical star ($\epsilon_I \to 0$) discussed in section 0.2. Solving the equations of motion for NS C the spherical components of the spin axis are given in figure 0.3.5. Both choices of χ yield a similar result, the polar angle a tends to χ on the spin down timescale as anticipated by the likeness to the spherical star. In contrast the azimuthal angle ϕ appears to begin monotonically increasing before approaching a constant, it is thought that this is due to the small but not vanishing magnitude of ϵ_I. In the perfectly spherical limit we observe no such increase in ϕ. Therefore the small deformation offsets the steady state solution of the spin axis from the magnetic dipole.

For an intuitive understanding consider that the torque acts to align the spin axis with the magnetic dipole; when this occurs the torque vanishes. Since the mass is not spherical, stable solutions exist only when the spin vector aligns with the principle axis of the moment of inertia tensor $\hat{\boldsymbol{x}}, \hat{\boldsymbol{y}}$ and $\hat{\boldsymbol{z}}$. So when both effects act, the steady state solution is an intermediary point between the two weighted by the relative strength of each effect. In this case the torque dominates and so the spin vector lies close, but not exactly aligned, with the magnetic dipole. During this time the star spins down but upon alignment the spin frequency asymptotically approaches a constant non zero value.
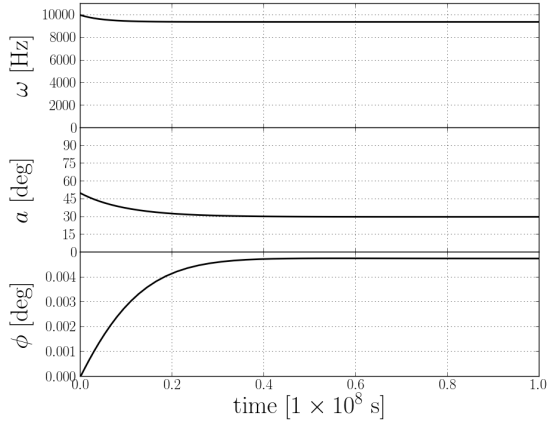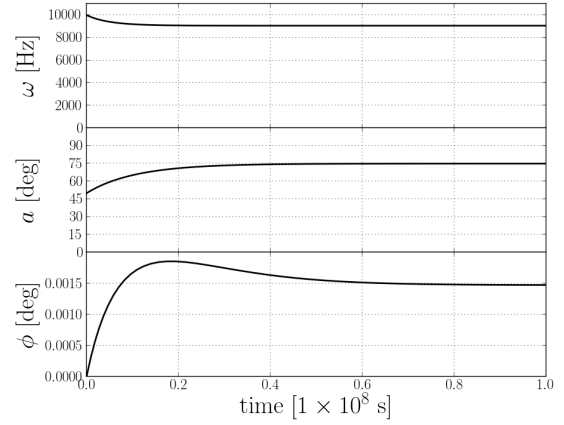
(a) $\chi = 30° < \chi_{cr}$ (b) $\chi = 75° > \chi_{cr}$

Figure 0.3.5: Plot of the spherical components of $\boldsymbol{\omega}$ for NS C.

0.4   Biaxial NS including the anomalous torque

We now include the anomalous torque component in equation (0.1.2) and discuss the differences this makes to the numerical solutions. Before doing this we consider the appropriate reference frame in which to view the system.

0.4.1   Effective body frame

Working with a biaxial body and the Deutsch torque Melatos (2000) discovered non-trivial solutions where the spin axis aligns with an unkown angle between the magnetic dipole and the principle axis of the MOI. This was interpreted by Melatos as evidence for persistent precession. We show in section 0.4.1 that in fact the spin vector is aligning with another rotating reference frame that is held at a fixed angle to the original rotating reference frame. This reference frame, which we label the *effective* body frame is a result of the inclusion of the anomalous torque.

Writing equation (0.1.2) with the Deutsch torque we have:

$$J^i_{,t} + \epsilon^{ijk}\omega_j J_k = N^i_{\text{spin down}} + \epsilon_A I_0 \omega^a \hat{m}_a \epsilon^{ijk}\omega_j \hat{m}_k,$$

$$J^i_{,t} + \epsilon^{ijk}\omega_j \left(J_k - \epsilon_A I_0 \omega^a \hat{m}_a \hat{m}_k\right) = N^i_{\text{spin down}},$$

$$J^i_{,t} + \epsilon^{ijk}\omega_j \left(I_{ka} - \epsilon_A I_0 \hat{m}_a \hat{m}_k\right)\omega^a = N^i_{\text{spin down}}.$$

By separating the equation this way and making use of $J_i = I_{ij}\omega^j$ we can write an effective moment of inertia tensor given by

$$
\begin{aligned}
I'_{jk} &= I_{jk} - I_0\epsilon_A \hat{m}_j \hat{m}_k, &(0.4.1)\\
&= \begin{bmatrix} I_0(1 - \epsilon_A \sin^2\chi) & 0 & -I_0\epsilon_A \sin\chi\cos\chi \\ 0 & I_0 & 0 \\ -I_0\epsilon_A \sin\chi\cos\chi & 0 & I_0(1 + \epsilon_I - \epsilon_A \cos^2\chi) \end{bmatrix}. &(0.4.2)
\end{aligned}
$$

9

Note we will use the prime to denote the effective body frame axis when quoting results. This effective moment of inertia tensor can be shown to have eigenvalues given by

$$\lambda_2 = I_0, \quad \lambda_\pm = \frac{I_0}{2} \left(2 + \epsilon_I - \epsilon_A \pm \sqrt{\epsilon_A^2 + \epsilon_I^2 - 2\epsilon_A \epsilon_I \cos(2\chi)} \right). \quad (0.4.3)$$

If we diagonalise this effective moment of inertia tensor, these eigenvalues are the diagonal entries, and the associated eigenvectors are the principle axis of the effective body frame axis. The eigenvalues always take the ordering

$$\lambda_+ > I_0 > \lambda_-. \quad (0.4.4)$$

Defining the effective body frame axis by e_i it is natural to associate the e_2 of the effective body frame axis with the $\hat{y}$ of the body frame axis such that they are always parallel. Since the other axis must be orthonormal, the transformation must consist of a rotation in the $x - z$ plane by an angle β. We are free to set the e_3 axis to always take the largest eigenvalue and then define β as the angle made by e_3 with the $\hat{z}$ axis. β is then given by:

$$\beta = \arctan \left(\frac{e_{3,1}}{e_{3,3}} \right) = \arctan \left(\frac{\epsilon_I - \epsilon_A \cos(2\chi) - \sqrt{\epsilon_A^2 + \epsilon_I^2 - 2\epsilon_A \epsilon_I \cos(2\chi)}}{2\epsilon_A \sin\chi \cos\chi} \right). \quad (0.4.5)$$

A schematic of the various angles and axis is given in figure 0.4.1
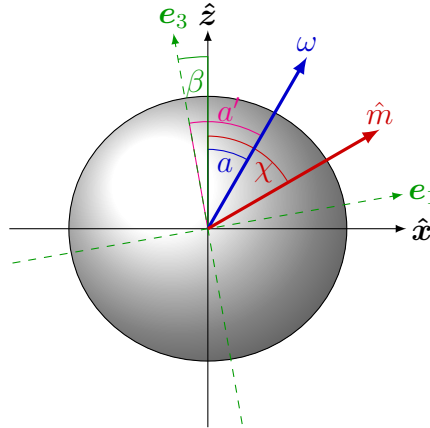

Figure 0.4.1: Schematic of the two sets of axis for an arbitary β. Note that β is defined to be positive for a right hand rotation about the $\hat{y}$ axis which is defined to be into the page.

Understanding the effective body frame The effective body frame is a simple rotation of the axis defined by the moment of inertia tensor to accommodate the effects of the anomalous torque. We work in a specialised case where the rotation is in only the $x - z$ plane by an angle β.

To understand when this becomes significant we plot β as a function of $|\epsilon_A/\epsilon_I|$ in figure 0.4.2. When $|\epsilon_A \ll \epsilon_I|$, such that the anomalous torque effects are negligible, we recover the usual moment of inertia tensor. That is, $\beta = 0$ or $\beta = \pi/2$, dependent on

the sign of ϵ_I. This is a consequence of choosing $\boldsymbol{e}_3$ to take the largest eigenvalue. In the opposing limit $|\epsilon_A \gg \epsilon_I|$, in which the magnetic deformation dominates the sign of the elastic deformation no longer splits the solutions and both cases tend to $\chi - 90°$. This means the effective body frame always aligns the $\boldsymbol{e}_1$ axis (which has the smallest eigenvalue) with the magnetic dipole.
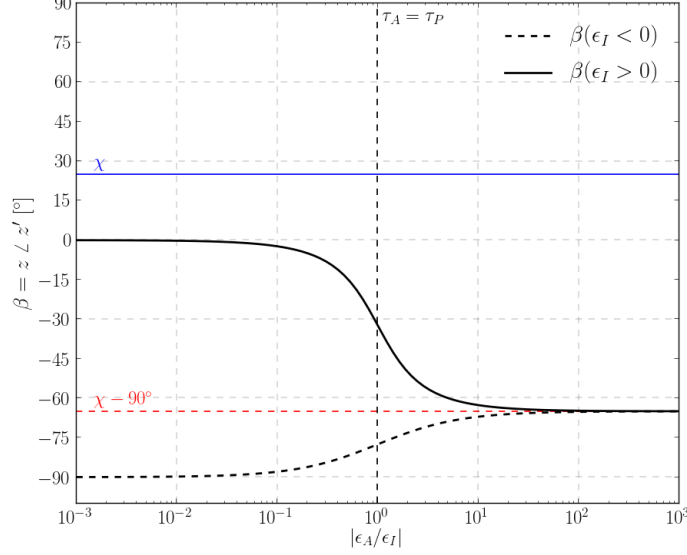

Figure 0.4.2: Plot of β as a function of the ratio $|\epsilon_A/\epsilon_I|$ for a prolate, $\epsilon_I < 0$ and oblate $\epsilon_I > 0$ mass distribution.

It should be made clear the rotation to the effective body frame is done in the post processing stage after the numerical ODEs are solved in the usual body frame. All three of our NSs have a non vanishing β, table 0.3.1 lists the relevant timescales and β for each NS.

NS	ϵ_I	ϵ_A	B_S [Gauss]	τ_S [s]	τ_A [s]	τ_P [s]	$\beta(\chi = 30°)$	$\beta(\chi = 75°)$
A	1.0×10^{-9}	5×10^{-9}	1.3×10^{13}	3.6×10^8	1.3×10^7	6.3×10^5	$-1.27°$	$-0.7°$
B	0.4×10^{-10}	5×10^{-9}	1.3×10^{13}	3.6×10^8	1.3×10^7	1.6×10^7	$-35.447°$	$-8.35°$
C	1.0×10^{-15}	5×10^{-9}	1.3×10^{13}	3.6×10^8	1.3×10^7	6.3×10^{11}	$-60.0°$	$-15.0°$

Table 0.4.1: Table of relevant values for the selected points.

Phase space

The introduction of the anomalous torque means we must also consider the anomalous torque timescale as given in equation (0.1.7). Three timescales can take six orderings. However, thhe spindown and anomalous timescale obey the following relation

$$\tau_S = \frac{3c}{2R}\frac{1}{\nu_0}\tau_A. \tag{0.4.6}$$

The coefficient $2R/3c$ effectively measures the importance of special relativity at the surface of the star. Since we expect $c \gg R\omega_0$ this means that only three physical orderings exist:

1. Region A: $\tau_S > \tau_A > \tau_P$

2. Region B: $\tau_S > \tau_P > \tau_A$

3. Region C: $\tau_P > \tau_S > \tau_A$

We can therefore update the phase space of possible solutions with the additional anomalous timescale; the result is given in figure 0.4.3.
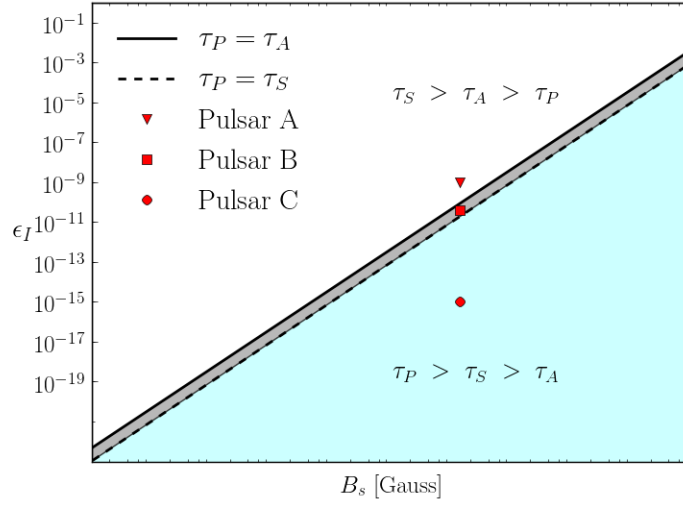

Figure 0.4.3: Phase space diagram including the anomalous torque contributions.

NS A in region $\tau_S > \tau_A > \tau_P$

We expect the alignment of the spin axis to agree with the findings in G70 and study the changes in behaviour due to the anomalous torque. Working in the effective body frame axis rotates the solutions by a few degrees as shown in table 0.4.1. Plotted in figure 0.4.4 are the spherical components of the spin vector in the effective body frame axis.

The final state alignment agrees well with previous results for both values of χ. For $\chi = 30°$ the intermediate behaviour appear similar to those shown in section 0.3.1. For $\chi = 75°$ we have what appears to be a large discontinuity in the solution suggesting a significant difference between solutions when including the anomalous torque. To understand the cause of this, we return to the geometric argument made in section 0.3.1
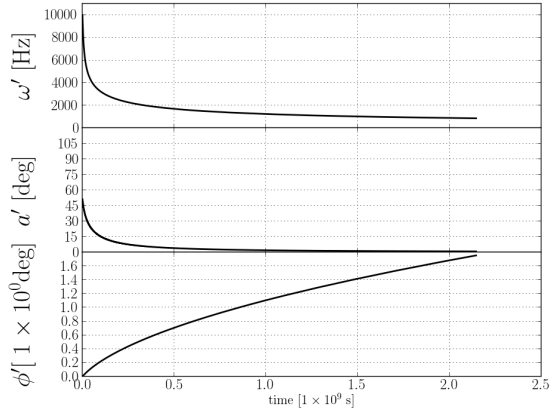
(a) $\chi = 30° < \chi_{cr}$
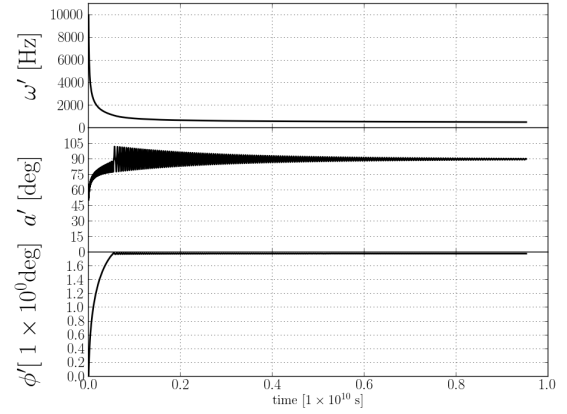
(b) $\chi = 70° > \chi_{cr}$

Figure 0.4.4: Plot of the spherical components of the spin vector during the spin down of NS A.

A geometric argument   Working in the effective body frame for which the effective moment of inertia tensor is triaxial. The conservation of angular momentum and conservation of energy are given by

$$1 = \frac{J_1^2}{2\lambda_- E} + \frac{J_2^2}{2I_0 E} + \frac{J_3^2}{2\lambda_+ E}. \tag{0.4.7}$$

$$J^2 = J_1^2 + J_2^2 + J_3^2. \tag{0.4.8}$$

The conservation of angular momentum describes an ellipsoid with semi axis given by $\sqrt{2\lambda_- E}$, $\sqrt{2I_0 E}$, and $\sqrt{2\lambda_+ E}$. The conservation of energy describes a sphere of radius J and for physical solutions the radius of the sphere is bounded by

$$2E\lambda_- < J^2 < 2E\lambda_+. \tag{0.4.9}$$

For a fixed energy and angular momentum we now have three distinct types of intersections as drawn in figure 0.4.5. We can now relate the three types of intersections to three types of solutions for the spin vector.

(a) $2E\lambda_- < J^2 < 2EI_0$ In this region curves form two sets of complete loops around the $\boldsymbol{e}_1$ axis. As $J^2 \to 2E\lambda_-$ the intersection loops will close up about the $\boldsymbol{e}_1$ axis.

(b) $J^2 = 2EI_0$ A special case in which the intersection forms two closed ellipses

(c) $2EI_0 > J^2 > 2E\lambda_+$ In this region curves form two sets of complete loops around the $\boldsymbol{e}_3$ axis. As $J^2 \to 2E\lambda_+$ the intersection loops will close up about the $\boldsymbol{e}_3$ axis.

13

(a) $2E\lambda_- < J^2 < 2EI_0$ (b) $J^2 = 2EI_0$ (c) $2EI_2 < J^2 < 2EI_3$
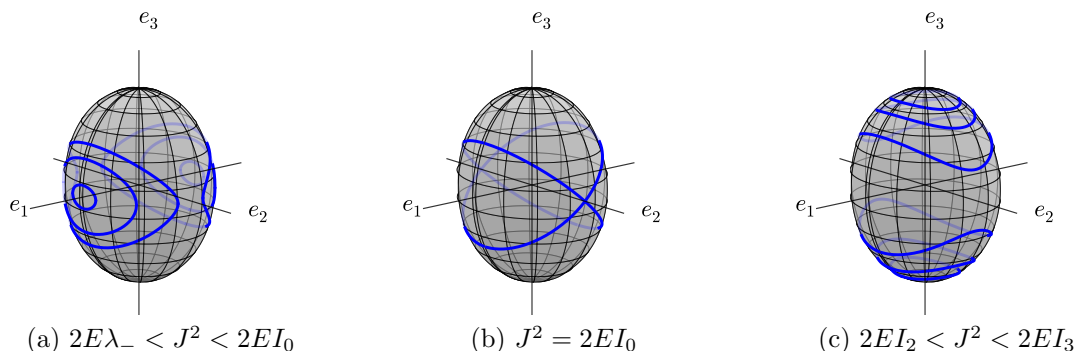
Figure 0.4.5: Intersection of the sphere and ellipsoid defined in equations (0.4.7) and (0.4.8) respectively.

All simulations begin in the same initial state. As previously observed, changing χ through the critical value changes the sign of $\dot{A}$ and hence whether the sphere will grow or shrink with respect to the ellipsoid. So for $\chi = 30°$ the sphere grows with respect to the ellipsoid ($\dot{A} > 0$) ending up with the loops closing up about the $\boldsymbol{e}_3$ axis. For $\chi = 75°$ the sphere shrinks with respect to the ellipsoid ($\dot{A} < 0$) ending up with the loops closing up about the $\boldsymbol{e}_1$ axis. The two end states are then the (a) and (c) pictures in figure 0.4.5.

If they both begin from the same initial configuration, then one of them must pass through the special $J^2 = 2EI_0$ state corresponding to figure 0.4.5. When this happens, we will observe a chnage in the axis about which the solution precesses.

Both sets of solution start with the solution precessing about the $\boldsymbol{e}_3$ axis (ϕ monotonically increasing) corresponding to figure 0.4.5(c) In figure 0.4.4(b) the discontinuity is in fact exactly the point when the solution changes the axes of precession.

To better understand this, we plot the data from the $\chi = 75°$ simulation (0.4.4(b)) in figure 0.4.6. Firstly in (a) we project the spherical components onto the unit sphere and choose three short sections of data. This shows that at early times, in blue, the solution precesses about the $\boldsymbol{e}_3$ axis. During the discontinuity, in red, the solution shows similarities with the $J^2 = 2EI_0$ case from figure 0.4.5. Finally at late times, in black, the solution precesses about the $\boldsymbol{e}_1$ axis. In figure 0.4.6(b) we also plot the solution in 3D during the apparent discontinuity. This again shows the solution goes through a change of the axis about which it precesses.
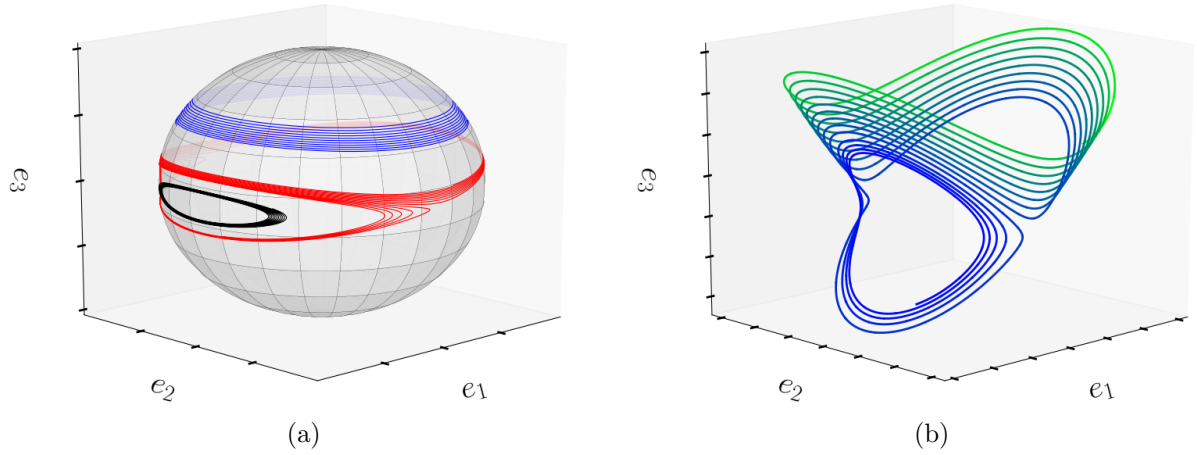
Figure 0.4.6: Numerical solutions for NS A plotted on the unit sphere in the body frame axis. (a) shows three distinct time steps: blue, the time before the discontinuity, red is during the discontinuity and black is some time after. (b) demonstrates the solution during the discontinuity, the changing colour is used to illustrate the evolution with time.

NS B in region $\tau_S > \tau_P > \tau_A$

This NS takes on a new significance having included the anomalous torque: we can now make a comparison with the work of Melatos (2000). In this work, Melatos found that when the precession timescale and anomalous torque timescales are comparable the solution admits persistent precession. This was defined as the polar angle a tending to a constant non-zero value with the nutation amplitude (oscillations in a) either decaying or remaining constant. Because the spin vector has not aligned with a principle axis of the moment of inertia this was interpreted as the spin vector undergoing persistent precession. Working in the body frame axis we confirm that $a \neq \pi/2$ at the end of the evolution in figure 0.4.7(a).

Transforming to the effective body frame in figure 0.4.7(b) we find that the spin vector in fact aligns with the principle axis of the effective moment of inertia ($a \to \pi/2$. Therefore the persistent precession angle found by Melatos is precisely the angle β. If the effective moment of inertia tensor is to be believed, then there is no persistent precession. The spin vector aligns aligns with the principle axis of the effective moment of inertia tensor associated with the smallest eigenvalue.
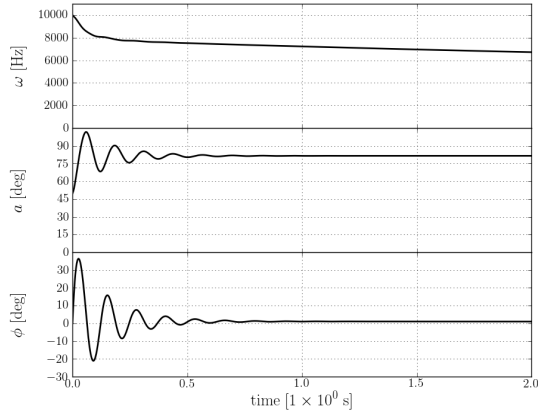
(a) In the body frame axis
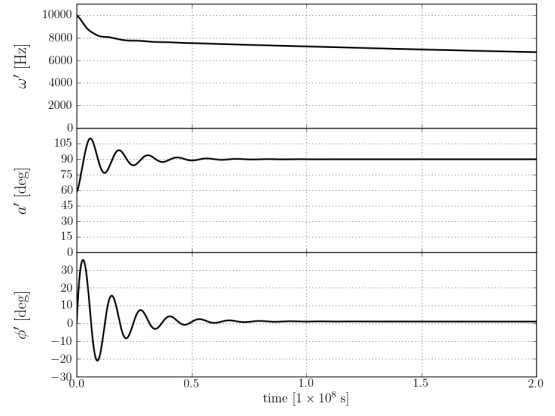
(b) In the effective body frame axis

Figure 0.4.7: Plot of the spherical components of $\boldsymbol{\omega}$ for NS B

NS C in region $\tau_P > \tau_S > \tau_A$

For all values of χ the spin vector is found to align with 1. In this limit ($\epsilon_A \gg \epsilon_I$ in figure 0.4.2) the $\boldsymbol{e}_1$ axis aligns with the magnetic dipole, this agrees with the results for a spherical star ($\epsilon_I \to 0$). The addition of the anomalous torque introduces oscillations on the anomalous torque timescale.
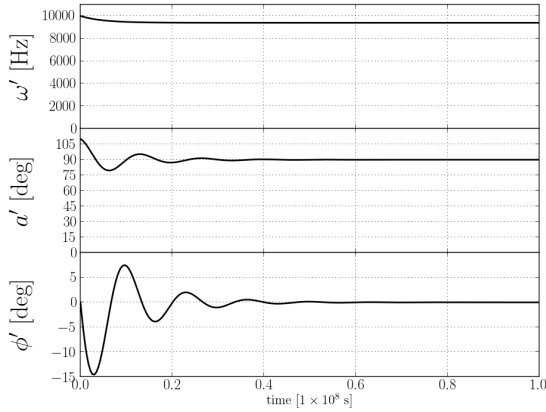
(a) $\chi = 30° < \chi_{cr}$
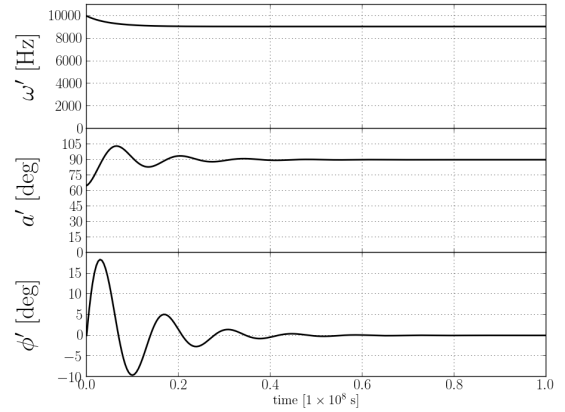
(b) $\chi = 75° > \chi_{cr}$

Figure 0.4.8: Plot of the spherical components of $\boldsymbol{\omega}$ for NS C.

0.4.2 Conclusion: Alignment of the spin vector

This simple model, comprising an elastic body supporting a biaxial strain and acted on by an electromagnetic torque, has been validated against known analytic results. Neglecting

the anomalous torque we expand on the results of Goldreich (1970): the dependency on χ of the spin vector alignment is related to the ratios of angular momentum and energy.

When using the anomalous torque we introduce the effective body frame. In all cases we find that the spin vector aligns with the principle axis of the effective moment of inertia tensor. For NSs in region A of figure 0.4.3 the effective moment of inertia tensor is triaxial. This means that it is possible for the spin vector to precess about either of the principle axis associated with the smallest and largest eigenvalue. As a result solutions can admit apparent discontinuities, under inspection these are revealed as the points where the precession changes between the two axis.

0.5 Connection with the known NS population

TBD

.A   Goldreich's result

Starting with

$$A = \frac{M^2}{2EI_0}, \tag{.A.1}$$

and differentiating

$$\dot{A} = \frac{1}{(2EI_0)^2}\left(\frac{d}{dt}(M^2)2EI_0 - \frac{d}{dt}(2EI_0)M^2\right), \tag{.A.2}$$

simplifying and writing in index notation we have

$$\dot{A} = \frac{1}{E^2}\left(2M^i\dot{M}_iE - \dot{E}M^iJ_i\right). \tag{.A.3}$$

Now $E = \frac{1}{2}I_{ij}\omega^i\omega^j$, $\dot{E} = T^i\omega_i$ and $\dot{M}^i = T^i$, and so

$$\dot{A} = \frac{1}{E^2}\left(M^iT_iI_{jk}\omega^j\omega^k - T^i\omega_iM^jJ_j\right). \tag{.A.4}$$

For a diagonalised matrix, I_{ij} has only 3 non zero components and so $I_{jk}\omega^j\omega^k = (I\omega)_j\omega^j$. In addition $M^i = (I\omega)^i$ and so writing

$$\dot{A} = \frac{1}{E^2}T^i\left((I\omega)_i\omega_j - \omega_i(I\omega)_j\right)(I\omega)^j, \tag{.A.5}$$

$$\dot{A} = \frac{1}{E^2}T^i\omega_i\omega_j(I\omega)^j\left(I^i_{\ i} - I^j_{\ j}\right). \tag{.A.6}$$

Considering for the time being only the last few terms and expanding the summation it is clear all $i = j$ terms will be zero. Working with a biaxial mass distribution where $I_1 = I_2$, then the only non-zero terms are given by

$$
\begin{aligned}
T^i\omega_i\omega_j(I\omega)^j\left(I^i_{\ i} - I^j_{\ j}\right) &= T_1\omega_1I_0(1-\epsilon_i)\omega_3^2(I_0 - I_0(1+\epsilon_I)) + T_2\omega_2I_0(1-\epsilon_i)\omega_3^2(I_0 - I_0(1+\epsilon_I)) \\
&\quad + T_3\omega_3(I_0(1+\epsilon_I) - I_0)(I_0\omega_1^2 + I_0\omega_2^2), \\
&= I_0^2\epsilon_I\omega_3\left(T_3(\omega_1^2 + \omega_2^2) - \omega_3(1+\epsilon_I)(T_1\omega_1 + T_2\omega_2)\right).
\end{aligned}
$$

Working up to 1st order in ϵ_I and inserting the spherical polar coordinates and then the spindown torque (we neglect the anomalous torque here) we have

$$
\begin{aligned}
&= I_0^2\epsilon_I\omega^3\left(\frac{2R}{3c}\epsilon A\omega^3\right)\cos a\left(\left[\sin\chi\cos\chi\sin a\cos\phi - \sin^2\chi\cos a\right]\sin^2 a\right. \\
&\quad \left. - \cos a([\sin\chi\cos\chi\sin a\cos\phi - \sin^2\chi\cos a]\cos\phi\sin a - \sin^2 a\sin^2\phi)\right).
\end{aligned}
$$

Of course to know the exact behaviour, one would need to fully solve the original ODEs. To show agreement with Goldreich's result, we can assume that ϕ varies much faster than a and ω such that $\tau_P << \tau_S$. Then averaging over a free nutation period and neglecting the coefficients for the time being

$$
\begin{aligned}
&\sim \cos a\left(-\sin^2 a\cos a\sin^2\chi + \frac{1}{2}\left(\sin^2 a\cos a\cos^2\chi + \sin^2 a\cos a\right)\right) \\
&\sim \cos^2 a\sin^2 a\left(1 - \frac{3}{2}\sin^2\chi\right).
\end{aligned}
$$

Finally putting all the terms together we have an expression for the averaged rate of change of A with respecting Goldreich's assumptions:

$$\langle \dot{A} \rangle = \frac{1}{\langle E \rangle^2} I_0^2 \epsilon_I \omega^6 \frac{2R}{3c} \epsilon A \cos^2 a \sin^2 a \left(1 - \frac{3}{2} \sin^2 \chi \right) \tag{.A.7}$$

.B   Considerations for the timescales

We have used the ordering of the three timescale at $\omega_0 = \omega(t = 0)$ to categorise the results. However, clearly the magnitude of the spin vector will decrease and the different dependencies on the spin vector could cause a 'crossing' of the timescales producing unexpected results. Writing the timescales then as

$$\tau_P(t) = \frac{2\pi}{\epsilon_I \omega(t)}, \quad \tau_A(t) = \frac{2\pi}{\epsilon_A \omega(t)}, \quad \tau_S(t) = \frac{3c}{2R} \frac{2\pi}{\epsilon_A \omega(t)^2}. \tag{.B.1}$$

Only τ_S could cross with the other two timescales since the spin down and anomalous timescales obey $\tau_S > \tau_A$ provided that

$$\omega(t) > \frac{3c}{2R}.$$

This condition is satisfied by setting the initial rotational spin frequency at less than $\omega_0 \sim 10^4$ [Hz rad], that is the star should not break special relativity. At later times the spin frequency will decay and so this condition is still satisfied.

For the anomalous torque and precession timescale crossings two cases exists: either the deformations are such that the spin down timescale is larger than the precession initially (region A and B) or, as in region C, the precession timescale is larger than then spin down timescale. Considering the first case:

$$\tau_S > \tau_P \quad \Rightarrow \omega(t) < \frac{3c}{2R} \frac{\epsilon_I}{\epsilon_A}. \tag{.B.2}$$

In this particular state $\epsilon_I > \epsilon_A$ and so as in the previous case while the spin vector decays this inequality is always satisfied and the orderings remain the same. In the other case we have:

$$\tau_P > \tau_S \quad \Rightarrow \omega(t) > \frac{3c}{2R} \frac{\epsilon_I}{\epsilon_A}. \tag{.B.3}$$

In this case it is possible for the time scales to cross at $\omega_{cr} = \frac{3c}{2R} \frac{\epsilon_I}{\epsilon_A}$. For pulsar C this corresponds to a rotational spin frequency of 0.9 [Hz rad] which is four orders of magnitude smaller than the initial freuquency. For this reason we can rule out this crossing of the time scales as an important factor in calculations.

Bibliography

Davis, L. and Goldstein, M. (1970). Magnetic-dipole alignment in pulsars. *The Astrophysical Journal*, 159.

Deutsch, A. (1955). The electromagnetic field of an idealized star in rigid rotation in vacuo. *Annales d'Astrophysique*.

Glampedakis, K. and Jones, D. I. (2010). Implications of magnetar non-precession. *Monthly Notices of the Royal Astronomical Society: Letters*, 405(1):L6–L10.

Goldreich, P. (1970). Neutron star crusts and alignment of magnetic axes in pulsars. *The Astrophysical Journal*.

Landau, L. D. and Lifshitz, E. M. (1969). *Mechanics*. Pergamon press.

Melatos, A. (2000). Radiative precession of an isolated neutron star. *Monthly Notices of the Royal Astronomical Society*, 313(2):217–228.

Michel, F. C. and Goldwire, Jr., H. C. (1970). Alignment of Oblique Rotators. In *Bulletin of the American Astronomical Society*, volume 2 of *Bulletin of the American Astronomical Society*, page 209.

Shapiro, S. L. and Teukolsky, S. A. (1983). *Black Holes, White Dwarfs, and Neutron Stars*. John Wiley & Sons, Inc.